THE Hα LUMINOSITY FUNCTION AND STAR FORMATION RATE AT $Z \approx 0.24$ IN THE COSMOS 2 SQUARE-DEGREE FIELD[1]

Y. Shioya [2], Y. Taniguchi [2], S. S. Sasaki [2, 3, 5], T. Nagao [4], T. Murayama [3], M. I. Takahashi [3], M. Ajiki [3], Y. Ideue [2], S. Mihara [2], A. Nakajima [2], N. Z. Scoville [5, 6], B. Mobasher [7], H. Aussel [6,8], M. Giavalisco [7], L. Guzzo [9], G. Hasinger [10], C. Impey [11], O. LeFevre [12], S. Lilly [13], A. Renzini [14], M. Rich [15], D. B. Sanders [6], E. Schinnerer [16], P. Shopbell [5], A. Leauthaud [12], J.-P. Kneib [5,12], J. Rhodes [5], and R. Massey [5,17]

Draft version February 1, 2008

ABSTRACT

To derive a new Hα luminosity function and to understand the clustering properties of star-forming galaxies at $z \approx 0.24$, we have made a narrow-band imaging survey for Hα emitting galaxies in the HST COSMOS 2 square degree field. We used the narrow-band filter NB816 ($\lambda_c = 8150$ Å, $\Delta\lambda = 120$ Å) and sampled Hα emitters with $EW_{\rm obs}({\rm H}\alpha + [{\rm NII}]) > 12$ Å in a redshift range between $z = 0.233$ and $z = 0.251$ corresponding to a depth of 70 Mpc. We obtained 980 Hα emitting galaxies in a sky area of 5540 arcmin^2, corresponding to a survey volume of 3.1×10^4 Mpc^3. We derive a Hα luminosity function with a best-fit Schechter function parameter set of $\alpha = -1.35^{+0.11}_{-0.13}$, $\log\phi_* = -2.65^{+0.27}_{-0.38}$, and $\log L_*({\rm erg~s}^{-1}) = 41.94^{+0.38}_{-0.23}$. The Hα luminosity density is $2.7^{+0.7}_{-0.6} \times 10^{39}$ ergs s^{-1} Mpc^{-3}. After subtracting the AGN contribution (15 %) to the Hα luminosity density, the star formation rate density is evaluated as $1.8^{+0.7}_{-0.4} \times 10^{-2}$ $M_\odot$ yr^{-1} Mpc^{-3}. The angular two-point correlation function of Hα emitting galaxies of $\log L({\rm H}\alpha) > 39.8$ is well fit by a power law form of $w(\theta) = 0.013^{+0.002}_{-0.001}\theta^{-0.88\pm0.03}$, corresponding to the correlation function of $\xi(r) = (r/1.9{\rm Mpc})^{-1.88}$. We also find that the Hα emitters with higher Hα luminosity are more strongly clustered than those with lower luminosity.

Subject headings: galaxies: distances and redshifts — galaxies: evolution — galaxies: luminosity function, mass function

1. INTRODUCTION

It is important to understand when and where intense star formation occurred during the course of galaxy evolution. Although the star formation history in individual galaxies is interesting, a general trend of star formation in galaxies as a function of time (or redshift) also provides important insights on the global star formation history as well as on the metal enrichment history in the universe. Therefore, the star formation rate density (SFRD) is one of the important observables for our understanding of galaxy formation and evolution. In the last decade, many works have followed the pioneer work of Madau et al. (1996) which compiled the evolution of SFRD, $\rho_{\rm SFR}$, as a function of redshift for the first time. The evolution of $\rho_{\rm SFR}$ is now widely accepted as follows: $\rho_{\rm SFR}$ steeply increases from $z \simeq 0$ to $z \sim 1$, and seems to be constant between $z \sim 2$ and $z \sim 5$ and may decline beyond $z \sim 5$ (Hopkins 2004 and references therein; Giavalisco et al. 2004; Taniguchi et al. 2005; Bouwens & Illingworth 2006).

Recent observations by the *Galaxy Evolution Explorer* (GALEX) and the *Spitzer Space Telescope* have confirmed that $\rho_{\rm SFR}$ increases from $z \sim 0$ to $z \sim 1$ (e.g., Schiminovich et al. 2005; Le Floc'h et al. 2005). However, their observations show that the IR luminosity density evolves as $(1+z)^4$ while the UV luminosity density evolves as $(1+z)^{2.5}$. This may imply that extinction by dust and reradiation from dust becomes to play a more important role at higher redshift. One of the remaining problems in this field is a relation between star-formation activity and large-scale structure formation. To study this issue, wide-field deep surveys are important.

There are several star formation rate (SFR) estimators, e.g., UV continuum, Hα emission, [OII] emission, far-infrared (FIR) emission (Kennicutt 1998), and radio continuum (Condon 1992). Each estimator has both advantage and disadvantage to estimate SFR. UV continuum and nebular emission lines are considered to be direct tracers of hot massive young stars. However, they

are often affected by dust obscuration. On the other hand, FIR and radio continuum are insensitive to dust obscuration. FIR emission is due to the dust heated by the general interstellar radiation field. If most of the bolometric luminosity of a galaxy absorbed by dust is radiated from young stars, as in the case of dusty starbursts, the FIR luminosity is a good SFR estimator. For early-type galaxies, much of the FIR emission is considered to be related to the old stars and the FIR emission is not a good SFR estimator (Sauvage & Thuan 1992; Kennicutt 1998). For star-forming galaxies, there is a tight radio-FIR correlation (Condon 1992). This relation suggests that the radio continuum also provides a good SFR estimator. The radio continuum is considered to be dominated by synchrotron radiation from relativistic electrons which are accelerated in supernova remnants (SNRs) (Lequeux 1971; Kennicutt 1983a; Gavazzi, Cocito, & Vettolani 1986). We note that the radio continuum emission of some galaxies is dominated by the AGN component, although such galaxies are distinguished from star-forming galaxies by using the tight radio-FIR correlation (Sopp & Alexander 1991; Condon 1992). The nearly linear radio-FIR correlation also suggests that radio continuum is affected by the efficiency of cosmic-ray confinement, since the degree of dust attenuation becomes larger for more luminous galaxies (Bell 2003). Although SFRs evaluated from different SFR estimators are consistent with each other within a factor of 3 if the appropriate correction is applied for each case (e.g., Hopkins et al. 2003; Charlot & Longhetti 2001; Charlot et al. 2002), samples selected with a different method may have different biases. For example, samples selected by an objective-prism imaging survey are biased toward the system with large equivalent width (e.g., Gallego et al. 1995), while those selected by UV radiation are biased against heavily dusty galaxies (Meurer et al. 2006). To evaluate the true SFRD, it is important to correct the obtained SFR appropriately and to know probable biases for the sample selection.

In this work, we use the Hα luminosity as a SFR estimator. The Hα luminosity is directly connected to the ionizing photon production rate. There are two approaches to measure Hα luminosities of galaxies. One is a spectroscopic survey and the other is a narrow-band imaging survey. Although spectroscopic observations tell us details of emission line properties, e.g., Balmer decrement, metallicity, and so on, it is difficult to obtain spectra of a large sample of faint galaxies. On the other hand, narrow-band imaging observations make it possible to measure an emission-line flux of galaxies over a wide field of view. Another advantage of narrow-band imaging is that aperture corrections dose not need to evaluate the total flux of Hα emission. However, there are some shortcomings in this method: e.g., narrow-band filter cannot separate Hα emission from [NII]$\lambda\lambda6548, 6583$ emission and we cannot evaluate the obscuration degree for each galaxy. Therefore, we must correct these effects statistically. Since the redshift coverage of emission-line galaxies discovered by the narrow-band imaging method is restricted, the survey volume of emission-line galaxies is small. Therefore, it is difficult to obtain a large sample of Hα emitters. If this is the case, brighter (i.e., rarer) Hα emitters could be missed in such an imaging survey. In order to study the Hα luminosity function unambigu-

ously, we need a large sample of Hα emitters covering a wide range of Hα luminosity. On the other hand, this restriction allows us to investigate large-scale structures of emission-line galaxies (mostly, star-forming galaxies) at a concerned redshift slice.

Motivated by this in part, we have carried out a narrow-band imaging survey of the HST COSMOS field centered at α(J2000)= $10^{\rm h}00^{\rm m}28.6^{\rm s}$ and δ(J2000)= $+02°12'21.0''$; the Cosmic Evolution Survey (Scoville et al. 2007). Since this field covers 2 square degree, it is suitable for our purpose. Our optical narrow-band imaging observations of the HST COSMOS field have been made with the Suprime-Cam (Miyazaki et al. 2002) on the Subaru Telescope (Kaifu et al. 2000; Iye et al. 2004). Since the Suprime-Cam consists of ten 2k×4k CCD chips and provides a very wide field of view ($34' \times 27'$), this is suitable for any wide-field optical imaging surveys. In our observations, we used the narrow-passband filter, $NB816$, centered at 8150 Å with the passband of $\Delta\lambda = 120$ Å. Our $NB816$ imaging data are also used to search both for Lyα emitters at $z \approx 5.7$ (Murayama et al. 2007) and for [OII] emitters at $z \approx 1.2$ (Takahashi et al. 2007). In this paper, we present our results on Hα emitters at $z \approx 0.24$ in the HST COSMOS field.

Throughout this paper, magnitudes are given in the AB system. We adopt a flat universe with $\Omega_{\rm matter} = 0.3$, $\Omega_\Lambda = 0.7$, and $H_0 = 70$ km s^{-1} Mpc^{-1}.

2. PHOTOMETRIC CATALOG

In this analysis, we use the COSMOS official photometric redshift catalog which includes objects whose total i magnitudes (i' or i^*) are brighter than 25. The catalog presents $3''$ diameter aperture magnitude of Subaru/Suprime-Cam B, V, r', i', z', and $NB816$ [18]. Details of the Suprime-Cam observations are given in Taniguchi et al. (2007). Details of the COSMOS official photometric redshift catalog is also described in Capak et al. (2007) and Mobasher et al. (2007). Since the accuracy of standard star calibration (±0.05 magnitude) is too large to obtain an accurate photometric redshift, Capak et al. (2007) re-calibrated the photometric zeropoints for photometric redshift using the SEDs of galaxies with spectroscopic redshift. Following the recommendation of Capak et al. (2007), we apply the zero-point correction to the photometric data in the official catalog. The offset values are 0.189, 0.04, -0.040, -0.020, 0.054, and -0.072 for B, V, r', i', z', and $NB816$, respectively. The zero-point corrected limiting magnitudes are $B = 27.4$, $V = 26.5$, $r' = 26.6$, $i' = 26.1$, $z' = 25.4$, and $NB816 = 25.6$ for a 3σ detection on a $3''$ diameter aperture. The catalog also includes $3''$ diameter aperture magnitude of CFHT i^*. We use the CFHT i^* magnitude for bright galaxies with $i' < 21$ because such bright galaxies appear to be slightly affected by the saturation effect in i' obtained with Suprime-Cam. We also apply the Galactic extinction correction adopting the median value $E(B - V) = 0.0195$ (Capak et al. 2007) for all objects. A photometric correction for each band is as follows (see Table 8 of Capak et al. 2007): $A_B = 0.079$,

---

[18] Our SDSS broad-band filters are designated as g^+, r^+, i^+, and z^+ in Capak et al. (2007) to distinguish from the original SDSS filters. Also, our B and V filters are designated as B_J and V_J in Capak et al. (2007) where J means Johnson and Cousins filter system used in Landolt (1992).

$A_V = 0.061$, $A_{r'} = 0.050$, $A_{i'} = 0.037$, $A_{z'} = 0.028$, $A_{NB816} = 0.034$, and $A_{i*} = 0.037$.

3. RESULTS

3.1. Selection of NB816-Excess Objects

We select Hα emitter candidates using $3''$ diameter aperture magnitude in the official catalog. In order to select NB816-excess objects efficiently, we need magnitude of frequency-matched continuum. Since the effective frequency of the NB816 filter (367.8 THz) is different either from those of i' (394.9 THz) and z' (333.6 THz) filters, we newly make a frequency-matched continuum, "iz continuum", using the following linear combination ; $f_{iz} = 0.57 f_{i'} + 0.43 f_{z'}$ where $f_{i'}$ and $f_{z'}$ are the i' and z' flux densities, respectively. Its $3\,\sigma$ limiting magnitude is $iz \simeq 26.03$ in a $3''$ diameter aperture. For the bright galaxies with $i' < 21$, "iz continuum" is calculated as $f_{iz} = 0.57 f_{i*} + 0.43 f_{z'}$, where f_{i*} is the $i*$ flux density, since i' magnitude is incorrect because of the saturation effect.

Since we use the ACS catalog prepared for studying weak lensing (Leauthaud et al. 2007) to separate galaxies from stars, our survey area is restricted to the area mapped in I_{814} band with Advanced Camera for Surveys (ACS) on HST. After subtracting the masked out area, the effective survey area is 5540 arcmin². Since the covered redshift range is between 0.233 and 0.251 ($\Delta z = 0.018$) and the corresponding survey depth is 70 Mpc, our effective survey volume is 3.1×10^4 Mpc³.

We selected NB816-excess objects using the following criteria:

$$iz - NB816 > 0.1, \qquad (1)$$

and

$$iz - NB816 > 3\sigma(iz - NB816), \qquad (2)$$

where

$$3\sigma(iz - NB816) = -2.5 \log(1 - \sqrt{(f_{3\sigma_{NB816}})^2 + (f_{3\sigma_{iz}})^2}/f_{NB816}) \qquad (3)$$

In the calculation of $3\sigma(iz - NB816)$, we applied the Galactic extinction correction to the limiting magnitudes of i'- and z'-band. The former criterion corresponds $EW_{obs} > 12$ Å. This criterion is exactly same as that of Fujita et al. (2003) and similar to that of Tresse & Maddox (1998) $[EW(\text{H}\alpha + [\text{O{\sc ii}}])_{rest} > 10$ Å$]$. Taking account of the scatter of $iz - NB816$ color, we added the latter criterion. These two criteria are shown by the solid and dashed lines, respectively, in Figure 1. As we will describe in the next section, we use the broad-band colors of galaxies to separate Hα emitters from other emission-line galaxies. To avoid the ambiguity of broad-band colors, we select galaxies detected above 3σ in all bands. Finally, we find 6176 galaxies that satisfy the above criteria.

3.2. Selection of NB816-Excess Objects at $z \approx 0.24$

The emission-line galaxy candidates selected above include not only Hα emitters at $z = 0.24$ but also possibly [O{\sc iii}] emitters at $z = 0.63$, or Hβ emitters at $z = 0.68$, or [O{\sc ii}] emitters at $z = 1.19$ (Tresse et al. 1999; Kennicutt 1992b). We also note here that the narrowband filter passband is too wide to separate [N{\sc ii}]$\lambda\lambda 6548, 6583$ from Hα.

In order to distinguish Hα emitters at $z \approx 0.24$ from emission-line objects at other redshifts, we investigate their broad-band color properties comparing observed colors of our 6176 emitters with model ones that are estimated by using the model spectral energy distribution derived by Coleman, Wu, & Weedman (1980). In Figures 2 & 3, we show the $B - V$ vs. $V - r'$ and $B - r'$ vs. $i' - z'$ color-color diagram of the 6176 sources and the loci of model galaxies. Then we find that Hα emitters at $z \approx 0.24$ can be selected by adopting the following three criteria; (1) $B - V > 2(V - r') - 0.2$, (2) $B - r' > 5(i' - z') - 1.3$, and (3) $B - r' > 0.7(i' - z') + 0.4$. We can clearly distinguish Hα emitters from [O{\sc iii}] or Hβ emitters using the first criterion. We can also distinguish Hα emitters from [O{\sc ii}] emitters using the second and third criteria. We have checked the validity of our photometric selection criteria using both the photometric data and spectroscopic redshifts of galaxies in the GOODS-N region (Cowie et al. 2004). Galaxies with redshifts corresponding to our Hα, [O{\sc iii}], Hβ, and [O{\sc ii}] emitters are separately plotted in Figs. 2 & 3. It is shown that our criteria can separate well Hα emitters from [O{\sc iii}], Hβ, and [O{\sc ii}] emitters. These criteria give us a sample of 981 Hα emitting galaxy candidates. The properties of GOODS-N galaxies presented in Figs. 2 and 3 suggest that there is few contamination in our Hα emitter sample.

3.3. Hα Luminosity

As we mentioned in section 1, one of the advantages of narrow-band imaging is to measure the total flux of Hα emission directly without any aperture correction. To derive the total Hα flux, we have used the total flux of i' (or $i*$), z', and NB816 using public images.[19] Our procedure is the same as that given in Capak et al. (2007); MAG_AUTO in SExtractor (Bertin & Arnouts 1996). Because of the contamination of the foreground galaxies, one galaxy has a negative value of $iz - NB816$ based on the total magnitudes. We do not use this object in further analysis. Therefore, our final sample contains 980 Hα emitters.

Adopting the same method as that used by Pascual et al. (2001), we express the flux density in each filter band as the sum of the line flux, F_L, and the continuum flux density, f_C:

$$f_{NB} = f_C + \frac{F_L}{\Delta NB}, \qquad (4)$$

$$f_{i'} = f_C + \frac{F_L}{\Delta i'}, \qquad (5)$$

and

$$f_{z'} = f_C, \qquad (6)$$

where ΔNB and $\Delta i'$ are the effective bandwidths of NB816 and i', respectively. The iz continuum, f_{iz}, is expressed as

$$f_{iz} = 0.57 f_{i'} + 0.43 f_{z'} = f_C + 0.57 \frac{F_L}{\Delta i'}. \qquad (7)$$

Using equation 4 and 7, the line flux F_L is calculated by

$$F_L = \Delta NB \frac{f_{NB} - f_{iz}}{1 - 0.57(\Delta NB / \Delta i')}. \qquad (8)$$

The line flux evaluated above includes both Hα and [N{\sc ii}]$\lambda\lambda 6548, 6583$ emission since the narrow-band filter

---

[19] http://irsa.ipac.caltech.edu/data/COSMOS/

cannot separate the contribution of these lines. The flux of Hα emission line is also affected by the internal extinction. Therefore, we have to correct the contamination of [NII]λλ6548, 6583 emission and the internal extinction $A_{\mathrm{H}\alpha}$. Although several correction methods have been proposed (e.g., Kennicutt 1992a; Gallego et al. 1997; Tresse et al. 1994; Helmboldt et al. 2004 for [NII] contamination: Kennicutt 1983b; Niklas et al. 1997; Kennicutt 1998; Hopkins et al. 2001; Afonso et al. 2003 for $A_{\mathrm{H}\alpha}$), there is few study which gives both corrections based on a single sample of galaxies. Helmboldt et al. (2004) have derived the relation between [NII]/Hα and M_R and that between $A_{\mathrm{H}\alpha}$ and M_R based on the data of the Nearby Field Galaxy Survey (Jansen et al. 2000a, 2000b). We therefore adopt their relations to correct the [NII] contamination and $A_{\mathrm{H}\alpha}$. After correcting to the AB magnitude system (Meurer et al. 2006), the relation between [NII]/Hα and M_R is

$$\log w_{6583} = -0.13 M_R - 3.30, \qquad (9)$$

where

$$w_{6583} \equiv \frac{F_{\mathrm{[NII]6583\mathring{A}}}}{F_{\mathrm{H}\alpha}} \qquad (10)$$

and that between $A_{\mathrm{H}\alpha}$ and M_R is

$$\log A_{\mathrm{H}\alpha} = -0.12 M_R - 2.47. \qquad (11)$$

To derive M_R used in equations (9) & (11) for each galaxy, we assume that the redshift of the galaxy is $z = 0.242$. We have also calculated k-correction using the average SED of Coleman et al. (1980)'s Sbc and Irr. Taking account of the luminosity distance and k-correction (average value of Scd and Irr), M_R is calculated from r'-band total magnitude, r', as $M_R = r' - 40.90$.

In addition to the above corrections, we also apply a statistical correction (21%; the average value of flux decrease due to the filter transmission) to the measured flux because the filter transmission function is not square in shape (Fujita et al. 2003). Note that this value is slightly different from that (28 %) used in Fujita et al. (2003). Our new value is re-estimated by using the latest filter response function. The Hα flux is given by:

$$F_{\mathrm{cor}}(\mathrm{H}\alpha) = F_{\mathrm{L}} \times \frac{f(\mathrm{H}\alpha)}{f(\mathrm{H}\alpha) + f([\mathrm{NII}])} \times 10^{0.4 A_{\mathrm{H}\alpha}} \times 1.21. \qquad (12)$$

Finally the Hα luminosity is estimated by $L(\mathrm{H}\alpha) = 4\pi d_{\mathrm{L}}^2 F_{\mathrm{cor}}(\mathrm{H}\alpha)$. In this procedure, we assume that all the Hα emitters are located at $z = 0.242$ that is the redshift corresponding to the central wavelength of our $NB816$ filter. Therefore, the luminosity distance is set to be $d_{\mathrm{L}} = 1213$ Mpc.

We summarize the total magnitude of i', z', $NB816$, and iz and the color excess of $iz - NB816$ for our Hα emission-line galaxy candidates in Table 1. Table 1 also includes $\log F_{\mathrm{L}}$, $\log F_{\mathrm{cor}}(\mathrm{H}\alpha)$, and $\log L(\mathrm{H}\alpha)$.

4. DISCUSSION

4.1. Luminosity function of Hα emitters

Figure 4 shows the Hα luminosity function (LF) at $z \approx 0.24$ for our Hα emitter sample. The Hα LF is constructed by the relation

$$\Phi(\log L_i) = \frac{1}{\Delta \log L} \sum_j \frac{1}{V_j} \qquad (13)$$

with

$$|\log L_j - \log L_i| < \frac{1}{2} \Delta \log L, \qquad (14)$$

where V_j is the volume of the narrow band slice in the range of redshift covered by the filter. We have used $\Delta \log L(\mathrm{H}\alpha) = 0.2$. If the shape of the filter response is square, our survey volume is 3.1×10^4 Mpc^3. However, effective survey volume is affected by the shape of filter transmission curve. For example, since the transmission at 8092 Å is a half of the peak value, the color excess, $iz - NB816$, of an Hα emitter at $z = 0.233$ with $EW(\mathrm{H}\alpha + [\mathrm{NII}]) = 12$Å is observed as 0.05 which does not satisfy our selection criterion, $iz - NB816 > 0.1$. Taking account of the filter shape in the computation of the volume, the correction can be as large as 23 % for the faintest galaxies. Adopting the Schechter function form (Schechter 1976), we obtain the following best-fit parameters for our Hα emitters with $L(\mathrm{H}\alpha) > 10^{39.8}$ ergs s^{-1}; $\alpha = -1.35^{+0.11}_{-0.13}$, $\log \phi_* = -2.65^{+0.27}_{-0.38}$, and $\log L_*(\mathrm{erg\ s}^{-1}) = 41.94^{+0.38}_{-0.23}$ (black solid line).

Together with our Hα LF, Figure 4 shows Hα LFs of previous studies in which Hα emitters at $z < 0.3$ are investigated; Tresse & Maddox (1998) [which is characterized by $\alpha = -1.35$, $\phi_* = 10^{-2.56}$ Mpc^{-3}, and $L_* = 10^{41.92}$ ergs s^{-1}; note that these parameters were converted by Hopkins (2004) to those of our adopted cosmology], Fujita et al. (2003), Hippelein et al. (2003) and Ly et al. (2007). Fujita et al. (2003), Ly et al. (2007), and this work are based on the $NB816$ imaging obtained with the Subaru Telescope. Tresse & Maddox (1998) is based on the Canada-France Redshift Survey (CFRS) and Hippelein et al. (2003) is based on the Calar Alto Deep Imaging Survey (CADIS).

First, we compare our Hα LF with that derived by Ly et al. (2007). Their best-fit Schechter function parameters ($\alpha = -1.71$, $\log \phi_* = -3.7$, $\log L_* = 42.2$) are quite different from those of our Hα LF. However we note that the data points between $\log L(\mathrm{H}\alpha) \sim 39.5$ and ~ 41.0, shown in Fig.10b of Ly et al. (2007), are quite similar to our results (Figure 4). We therefore consider that the Hα LF of Ly et al. (2007) itself is basically consistent with ours except the brightest point. The difference of Schechter parameters between ours and Ly et al's may arise from the data points of the brightest and the faintest ones, especially the brightest one. Since the field of view of the COSMOS is about an order wider than that of the SDF, we consider that our Hα LF is more accurate by determined than that of Ly et al. (2007) at the bright end.

Second, we compare our Hα LF with the other Hα LFs. Although our Hα LF is similar to those of Tresse & Maddox (1998) and Hippelein et al. (2003), the Hα LF of Fujita et al. (2003) shows a steeper faint-end slope and a higher number density for the same luminosity than ours. These differences may be attributed to the following different source selection procedures: (1) Fujita et al. (2003) used their $NB816$-selected galaxies while we used i'-selected galaxies, Tresse & Maddox (1998) used I-selected Canada-France Redshift Survey (CFRS) galaxies, and Hippelein et al. (2003) used Fabry-Perot images for pre-selection of emission-line galaxies. As Fujita et al. (2003) demonstrated, samples based on a broad-band selected catalog are biased against galaxies with faint con-

tinuum. (2) Fujita et al. (2003) used their $B - R_{\rm C}$ vs. $R_{\rm C} - I_{\rm C}$ color - color diagram to isolate Hα emitters from other low-z emitters at different redshifts. However, we find that there are possible contaminations of [OIII] emitters if one uses the $B - R_{\rm C}$ vs. $R_{\rm C} - I_{\rm C}$ diagram, because of the small difference between Hα and [OIII] emitters on that color - color diagram. On the other hand, we used $B - V$ vs. $V - r'$ to isolate Hα emitters from [OIII] emitters. Due to the large separation between Hα emitters and [OIII] emitters on the $B - V$ vs. $V - r'$ diagram, we can reduce the contamination of [OIII] emitters. (3) Fujita et al. (2003) used population synthesis model GISSEL96 (Bruzual & Charlot 1993) to determine the criteria for selecting Hα emitters. To check the validity of the criterion, we compare colors of GOODS-N galaxies at $z \sim 0.24$, 0.63, 0.68 & 1.19 with model colors at corresponding redshifts based on GISSEL96 (Figure 5). Unfortunately, the predicted colors are slightly different from those of observed galaxies. We therefore redetermined the selection criteria using the SED of Coleman, Wu, & Weedman (1980) as

$$(B - R_{\rm C}) > 2.5(R_{\rm C} - I_{\rm C}) + 0.2.$$

If we adopt this revised criterion, the number of Hα emitters in the Fujita et al. (2003) is reduced by about 20 % (Figure 5). This is one reason why the number density of Hα emitters in Fujita et al. (2003) is higher than other surveys. Recently, Ly et al. (2007) pointed out that the fraction of [OIII] emitters in the Hα emitter sample of Fujita et al. (2003) may be about 50 % using the Hawaii HDF-N sources with redshifts observed as $NB816$-excess objects. The Hα LF of Fujita et al. (2003) reduced by 50 % appears to be quite similar to our Hα LF.

4.2. *Luminosity density and star formation rate density*

By integrating the luminosity function, i.e.,

$$\mathcal{L}(\mathrm{H}\alpha) = \int_0^\infty \Phi(L)L\,dL = \Gamma(\alpha + 2)\phi_* L_*, \qquad (15)$$

we obtain a total Hα luminosity density of $2.7^{+0.7}_{-0.6} \times 10^{39}$ ergs s^{-1} Mpc^{-3} at $z \approx 0.24$ from our best fit LF. The star formation rate is estimated from the Hα luminosity using the relation $SFR = 7.9 \times 10^{-42}L(\mathrm{H}\alpha)$ $M_\odot \mathrm{yr}^{-1}$, where $L(\mathrm{H}\alpha)$ is in units of ergs s^{-1} (Kennicutt 1998). Using this relation, the Hα luminosity density can be translated into the SFR density of $\rho_{\rm SFR} \simeq 2.1^{+1.0}_{-0.4} \times 10^{-2} M_\odot$ yr^{-1} Mpc^{-3}.

However, not all the Hα luminosity is produced by star formation, because active galactic nuclei (AGNs) can also contribute to the Hα luminosity. For example, previous studies obtained the following estimates; 8-17% of the galaxies in the CFRS low-z sample (Tresse et al. 1996), 8% in the Universidad Complutense de Madrid (UCM) survey of local Hα emission line galaxies (Gallego et al. 1995), and 17-28% in the 15R survey (Carter et al. 2001). Recently, Hao et al. (2005) obtained an Hα luminosity function of active galactic nuclei based on the sample of the Sloan Digital Sky Survey within a redshift range of $0 < z < 0.15$. The Hα luminosity density calculated from Schechter function parameters which are shown in the paper is 1.1×10^{38} erg s^{-1} Mpc^{-3} (with no reddening correction). Taking account of the reddening correction and the Hα luminosity density radiated from

star-forming galaxies (Gallego et al. 1995), the fraction of AGN contribution to the total Hα luminosity density is about 15 % in the local universe. If we assume that the 15 % of the Hα luminosity density is radiated from AGNs, the corrected SFRD is $1.8^{+0.7}_{-0.4} \times 10^{-2}$ $M_\odot$ yr^{-1} Mpc^{-3}.

We note here that the error to $\rho_{\rm SFR}$ (and $\mathcal{L}(\mathrm{H}\alpha)$) is probably underestimated, since it does not include the effect of different correction methods and selection biases. For example, adopting the different relation for correcting $A_{\mathrm{H}\alpha}$ may cause a different value of SFRD.

We compare our result with the previous investigations compiled by Hopkins (2004) in Figure 6. We also show the evolution of SFRD derived from the observation of GALEX with mean attenuation of $A_{\rm UV}^{\rm meas} = 1.8$, evaluated from the FUV slope β ($f_\lambda \propto \lambda^\beta$) and the relation of $A_{\rm FUV} = 4.43 + 1.99\beta$. If we adopt the more representative value $A_{\rm UV}^{\rm min} = 1$ (Schiminovich et al. 2005) determined by using the $F_{\rm dust}/F_{\rm UV}$ ratio (Buat et al. 2005), their SFRD becomes smaller by a factor of 2, being similar to our SFRD.

The left panel of Figure 6 shows the evolution of the SFRD as a function of redshift from $z = 0$ to $z = 2$. The right panel of Figure 6 shows that as a function of the look-back time. It clearly shows that SFRD monotonically decreasing for 10 Gyr with increasing cosmic time. We note that the error of SFRD of our evaluation includes only random error, since we adopt the same assumptions as those in Hopkins (2004).

Our SFRD evaluated above seems roughly consistent with but slightly smaller than the previous evaluations, e.g., Tresse & Maddox (1998) and Fujita et al. (2003). Since we select emission-line galaxies with $EW(\mathrm{H}\alpha + [\mathrm{NII}])_{\rm obs} > 12$ Å, our sample is considered to be biased against star-forming galaxies with small specific SFR which is defined as the ratio of SFR to stellar mass of galaxy. Since our criterion is similar to that of Tresse & Maddox (1998) and the same as that of Fujita et al. (2003), we consider that the difference between our survey and theirs is not caused by the different criteria of $EW(\mathrm{H}\alpha + [\mathrm{NII}])_{\rm obs}$. As we mentioned in section 4.1, the SFRD of Fujita et al. (2003) was overestimated because of the contamination of [OIII] emitters. On the other hand, the difference between Tresse & Maddox (19989 and our work seems to be real; e.g., the cosmic variance.

We discuss further the effect of the selection criterion of $EW(\mathrm{H}\alpha + [\mathrm{NII}])_{\rm obs} > 12$ Å on the evaluation of SFRD. Being different from the previous Hα emission-line galaxy surveys using the objective-prism, the fraction of galaxies having $EW(\mathrm{H}\alpha) > 50$ Å is 12 % in our sample, which is similar to or less than the value of the local universe (15-20 %: Heckman 1998) and SINGG SR1 (14.5 %: Hanish et al. 2006). On the other hand, the fractions of the galaxies with $EW(\mathrm{H}\alpha) > 50$ Å are 42 % and 35 % in the KPNO International Spectroscopic Survey (KISS) (Gronwall et al. 2004) and UCM objective-prism surveys, respectively. Our sample seems to be not strongly biased toward galaxies with high equivalent width. Hanish et al. (2006) showed that 4.5 % of the Hα luminosity density comes from galaxies with $EW(\mathrm{H}\alpha) < 10$ Å in local universe. If the fraction (4.5 %) is valid for the star-forming galaxies at $z \approx 0.24$, our estimate of SFRD would be about 5 % smaller than the true SFRD.

4.3. Spatial Distribution and Angular Two-Point Correlation Function

Figure 7 shows the spatial distribution of our 980 Hα emitter candidates. There are some clustering regions over the field. To discuss the clustering properties more quantitatively, we derive the angular two-point correlation function (ACF), $w(\theta)$, using the estimator defined by Landy & Szalay (1993),

$$w(\theta) = \frac{DD(\theta) - 2DR(\theta) + RR(\theta)}{RR(\theta)}, \qquad (16)$$

where $DD(\theta)$, $DR(\theta)$, and $RR(\theta)$ are normalized numbers of galaxy-galaxy, galaxy-random, random-random pairs, respectively. The random sample consists of 100,000 sources with the same geometrical constraints as the galaxy sample. Figure 4 demonstrates that our Hα emitter sample is quite incomplete for $\log L(\mathrm{H}\alpha)(\mathrm{erg\ s}^{-1}) < 39.8$. We therefore show the ACF for 693 Hα emitter candidates with $\log L(\mathrm{H}\alpha)(\mathrm{erg\ s}^{-1}) > 39.8$ in Figure 8. The ACF is fit well by power law, $w(\theta) = 0.013^{+0.002}_{-0.001}\theta^{-0.88\pm0.03}$. Recently, the departure from a power-law of the correlation function is reported (Zehavi et al. 2004; Ouchi et al. 2005). Such departure may be interpreted as the transition from a large-scale regime, where the pair of galaxies reside in separate halos, to a small-scale regime, where the pair of galaxies reside within the same halo. We find no evidence for such departure in our result. We however consider that the number of our sample is too small to discuss this problem.

For Lyman break galaxies, brighter galaxies (with a larger star formation rate) tend to show more clustered structures than faint ones (with a smaller star formation rate) (e.g., Ouchi et al. 2004; Kashikawa et al. 2006). We also show the ACF of Hα emitters with larger Hα luminosity $[\log L(\mathrm{H}\alpha)(\mathrm{erg\ s}^{-1}) > 40.94 = \log(0.1L_*)]$ and that with lower Hα luminosity $(39.8 < \log L(\mathrm{H}\alpha)(\mathrm{erg\ s}^{-1}) \leq 40.94)$ in Figure 8. Both ACFs are well fit with a power law form: $w(\theta) = 0.019^{+0.004}_{-0.004}\theta^{-1.08\pm0.05}$ for objects with $\log L(\mathrm{H}\alpha)(\mathrm{erg\ s}^{-1}) > 40.94$, while $w(\theta) = 0.011^{+0.002}_{-0.002}\theta^{-0.84\pm0.05}$ for objects with $39.8 < \log L(\mathrm{H}\alpha)(\mathrm{erg\ s}^{-1}) \leq 40.94$, respectively. We conclude that galaxies with a higher star formation rate are more strongly clustered than ones with a lower star formation rate. This fact is interpreted as that galaxies with a higher star formation rate reside in more massive dark matter halos, which are more clustered in the hierarchical structure formation scenario.

It is useful to evaluate the correlation length r_0 of the two-point correlation function $\xi(r) = (r/r_0)^{-\gamma}$. A correlation length is derived from the ACF through Limber's equation (e.g., Peebles 1980). Assuming that the redshift distribution of Hα emitters is a top hat shape of $z = 0.242 \pm 0.009$, we obtain the correlation length of $r_0 = 1.9$ Mpc. Therefore, the two-point correlation function for all Hα emitters is written as $\xi(r) = (r/1.9\mathrm{Mpc})^{-1.88}$. The correlation length of Hα emitters with $\log L(\mathrm{H}\alpha)(\mathrm{erg\ s}^{-1}) > 40.94$ is 2.9 Mpc, while that

of Hα emitters with $39.8 < \log L(\mathrm{H}\alpha)(\mathrm{erg\ s}^{-1}) \leq 40.94$ is 1.6 Mpc. These values are smaller than those evaluated for nearby L_* galaxies (~ 7 Mpc) (Norberg et al. 2001; Zehavi et al. 2005) and $z \sim 1$ galaxies ($\sim 4 - 5$ Mpc)(Coil et al. 2004).

It is known that the correlation length is smaller for fainter galaxies in the nearby (Norberg et al. 2001; Zehavi et al. 2005) and the $z \sim 1$ universe (Coil et al. 2006). Figure 9 shows the relation between the $L(\mathrm{H}\alpha)$ and R_C-band absolute magnitude M_R for our sample. Our sample includes many faint ($M_R > -18$) galaxies. However, the correlation length for galaxies with $-18 < M_r < -17$ (3.8 Mpc: Zehavi et al. 2005) is still larger than that of our sample. This discrepancy may imply a weak clustering of emission-line galaxies.

5. SUMMARY

We have performed the Hα emitter survey in the HST COSMOS 2 square degree field using the COSMOS official photometric catalog. Our results and conclusions are summarized as follows.

1. We found 980 Hα emission-line galaxy candidates using the narrow-band imaging method. The Hα luminosity function is well fit by Schechter function with $\alpha = -1.35^{+0.11}_{-0.13}$, $\log \phi_* = -2.65^{+0.27}_{-0.38}$, and $\log L_*(\mathrm{erg\ s}^{-1}) = 41.94^{+0.38}_{-0.23}$. Using the parameter set of Schechter function, the Hα luminosity density is evaluated as $2.7^{+0.7}_{-0.6} \times 10^{39}$ erg s^{-1} Mpc^{-3}. If we adopt the AGN contribution to the Hα luminosity density is 15 %, we obtain the star formation rate density of $1.8^{+0.7}_{-0.4} \times 10^{-2} M_\odot \mathrm{yr}^{-1}\mathrm{Mpc}^{-3}$. This error includes only random error. Our result supports the strong increase in the SFRD from $z = 0$ to $z = 1$.

2. We studied the clustering properties of Hα emitters at $z \sim 0.24$. The two-point correlation function is well fit by power law, $w(\theta) = 0.013^{+0.002}_{-0.001}\theta^{-0.88\pm0.03}$, which leads to the correlation function of $(r/1.9\mathrm{Mpc})^{-1.88}$. We cannot find the departure from a power law, which is recently found in both low- and high-z galaxies. Although the power of -1.88 is consistent with the power for nearby galaxies, the derived correlation length of $r_0 = 1.9$ Mpc is smaller than that for nearby galaxies with the same optical luminosity range. This discrepancy may imply a weak clustering of emission-line galaxies. The galaxies with higher SFR are more strongly clustered than those with lower SFR. Taking account of the fact that the SFR of a luminous galaxy is higher than that of a faint galaxy, this result is consistent with the fact already known that the luminous galaxies are more strongly clustering.

REFERENCES

Afonso, J., Hopkins, A., Mobasher, B., & Almeida, C. 2003, ApJ, 597, 269

Bertin, E., & Arnouts, S. 1996, A&AS, 117, 393

TABLE 1
A LIST OF Hα EMITTER CANDIDATES.

#	ID	RA (deg)	DEC (deg)	i' (mag)	z' (mag)	$NB816$ (mag)	iz (mag)	$iz - NB816$ (mag)	$\log F_{\rm L}$ (erg s^{-1} cm^{-2})	$\log F_{\rm cor}$ (erg s^{-1} cm^{-2})	$\log L({\rm H}\alpha)$ (erg s^{-1})	$EW_{\rm obs}$ (Å)
1	58612	150.72533	1.611834	20.99	20.92	20.86	20.96	0.10	-16.11	-15.81	40.44	12
2	62649	150.67970	1.594458	20.89	20.64	20.64	20.78	0.13	-15.88	-15.57	40.67	17
3	101151	150.46013	1.600051	21.05	21.05	20.93	21.05	0.12	-16.05	-15.76	40.49	14
4	135016	150.33841	1.622284	22.98	22.58	22.70	22.79	0.09	-16.87	-16.67	39.58	11
5	137365	150.32673	1.605641	23.01	22.91	22.84	22.96	0.13	-16.78	-16.58	39.67	16

The complete version of the this table is in the electric edition of the Journal. The printed edition contains only a sample.

Bell, E. F. 2003, ApJ, 586, 794
Bouwens, R. J., & Illingworth, G. D. 2006, Nature, 443, 189
Bruzual A., G., & Charlot, S. 1993, ApJ, 405, 538
Buat, V. et al. 2005, ApJ, 619, L51
Capak, P., et al. 2007, ApJS in press
Carter, B. J., Fabricant, D. G., Geller, M. J., Kurtz, M. J., & McLean, B. 2001, 559, 606
Charlot, S., & Longhetti, M. 2001, MNRAS, 323, 887
Charlot, S., Kauffmann, G., Longhetti, M., Tresse, L., White, S. D. M., Maddox, S. J., & Fall, S. M. 2002, MNRAS, 330, 876
Coil, A. L., et al. 2004, ApJ, 609, 525
Coil, A. L., et al. 2006, ApJ, 644, 671
Coleman, G. D., Wu, C.-C., & Weedman, D. W. 1980, ApJS, 43, 393
Condon, J. J. 1992, ARAA, 30, 575
Connolly, A. J., Szalay, A. S., Dickinson, M., Subbarao, M. U., & Brunner, R. J. 1997, ApJ, 486, L11
Cowie, L. L., Songaila, A., & Barger, A. J. 1999, AJ, 118, 603
Cowie, L. L., Barger, A. J., Hu, E. M., Capak, P., & Songaila, A. 2004, AJ, 127, 3137
Fujita, S. S., et al. 2003, ApJ, 586, L115
Gallego, J., Zamorano, J., Aragón-Salamanca, A., & Rego, M. 1995, ApJ, 455, L1; Erratum 1996, ApJ, 459, L43
Gallego, J., Zamorano, J., Rego, M., & Vitores, A. G. 1997, ApJ, 475, 502
Gallego, J., García-Dabó, C. E., Zamorano, J., Aragón-Salamanca, A., & Rego, M. 2002, ApJ, 570, L1
Gavazzi, G., Cocito, A., & Vettolani, G. 1986, ApJ, 305, L15
Giavalisco, M., et al. 2004, ApJ, 600, L103
Glazebrook, K., Blake, C., Economou, F., Lilly, S., & Colless, M. 1999, MNRAS, 306, 843
Gronwall, C., Salzer, J. J., Sarajedini, V. L., Jangren, A, Chomiuk, L., Moody, J. W., Frattare, L. M., Boroson, T. A. 2004, AJ, 127, 1943
Gunn, J. E., & Stryker, L. L. 1983, ApJS, 52, 121
Hammer, F., et al. 1997, ApJ, 481, 49
Hanish, D. J., et al. 2006, ApJ, 649, 150
Hao, L., et al. 2005, AJ, 129, 1795
Helmboldt, J. F., Walterbos, R. A. M., Bothun, G. D., O'Neil, K., & de Blok, W. J. G. 2004, ApJ, 613, 914
Hippelein, H., Maier, C., Meisenheimer, K., Wolf, C., Fried, J. W., von Kuhlmann, B., Kümmel, M., Phleps, S., Röser, H.-J. 2003, A&A, 402, 65
Hogg, D. W., Cohen, J. G., Blandford, R., & Pahre, M. A. 1998, ApJ, 504, 622
Hopkins, A. M. 2004, ApJ, 615, 209
Hopkins, A. M., Connolly, A. J., & Szalay, A. S. 2000, AJ, 120, 2843
Hopkins, A. M., Connolly, A. J., Haarsma, D. B., & Cram, L. E. 2001, AJ, 122, 288
Hopkins, A. M., et al. 2003, ApJ, 599, 971
Iwamuro, F., et al. 2000, PASJ, 52, 73
Iye, M., et al. 2004, PASJ, 56, 381
Jansen, R. A., Franx, M., Fabricant, D., & Caldwell, N. 2000a, ApJS, 126, 271
Jansen, R. A., Fabricant, D., Franx, M., & Caldwell, N. 2000b, ApJS, 126, 331
Kaifu, N., et al. 2000, PASJ, 52, 1
Kashikawa, N. 2006, ApJ, 637, 631

Kennicutt, R. 1983a, A&A, 120, 219
Kennicutt, R. 1983b, ApJ, 272, 54
Kennicutt, R. C. 1992a, ApJ, 388,310
Kennicutt, R. C. 1992b, ApJS, 79, 255
Kennicutt, R. C. 1998 ARA&A, 36, 189
Landolt, A. U. 1992, AJ, 104, 340
Landy, S. D., Szalay, A. S. 1993, ApJ, 412, 64
Leauthaud, A., et al. 2007, ApJS, in press (astro-ph/0702359)
Le Floc'h, E., et al. 2005, ApJ, 632, 169
Lequeux, J. 1971, A&A, 15, 42
Lilly, S. J., Le Fevre, O., Hammer, F., Crampton, D. 1996, ApJ, 460, L1
Ly, C., et al. 2007, ApJ, 657, 738
Madau, P., Ferguson, H. C., Dickinson, M. E., Giavalisco, M., Steidel, C. C., & Fruchter, A. 1996, MNRAS, 283, 1388
Massarotti, M., Iovino, A., & Buzzoni, A. 2001, ApJ, 559, L105
Meurer, G. R., et al. 2006, ApJS, 165, 307
Miyazaki, S., et al. 2002, PASJ, 54, 833
Mobasher, B., et al. 2007, ApJS, in press (astro-ph/0612344)
Moorwood, A. F. M.,van der Werf, P. P., Cuby, J. G., & Oliva, E. 2000, A&A, 362, 9
Murayama, T., et al. 2007, ApJS, in press (astro-ph/0702458)
Norberg, P., et al. 2001, MNRAS, 328, 64
Ouchi, M., et al. 2004, ApJ, 611, 685
Ouchi, M., et al. 2005, ApJ, 635, L117
Pascual, S., Gallego, J., Aragón-Salamanca, A., & Zamorano, J. 2001, A&A, 379, 798
Peebles, P. J. E. 1980, The Large-Scale Structure of the Universe, Princeton, N. J., Princeton Univ. Press
Pérez-González, P. G., Zamorano, J., Gallego, J., Aragón-Salamanca, A., & Gil de Paz, A. 2003, ApJ, 591, 827
Sauvage, M., & Thuan, T. X. 1992, ApJ, 396, L69
Schechter, P. 1976, ApJ, 203, 297
Schminovich, D., et al. 2005, ApJ, 619, L47
Scoville, N. Z., et al. 2007, ApJS, in press (astro-ph/0612305)
Sopp, H. M., & Alexander, P. 1991, MNRAS, 251, p.14
Sullivan, M., Treyer, M., Ellis, R. S., Bridges, B., & Donas, J. 2000, MNRAS, 312, 442
Takahashi, M., et al. 2007, submitted to ApJS
Taniguchi, Y., et al. 2005, PASJ, 57, 165
Taniguchi, Y., et al. 2007, ApJS, in press (astro-ph/0612295)
Teplitz, H. I., Collins, N. R., Gardner, J. P., Hill, R. S., & Rhodes, J. 2003, ApJ, 589, 704
Tresse, L., & Maddox, S. 1998, ApJ, 495, 691
Tresse, L., Maddox, S., Le Fèver, O., & Cuby, J.-G. 2002, MNRAS, 337, 369
Tresse, L., Maddox, S., Loveday, J., & Singleton, C. 1999, MNRAS, 310, 262
Tresse, L., Rola, C., Hammer, F., Stasińska, G., Le Fèvre, O., Lilly, S. J., & Crampton, D. 1996, MNRAS, 281, 847
Treyer, M. A., Ellis, R. S., Milliard, B., Donas, J., & Bridges, T. J. 1998, MNRAS, 300, 303
Wilson, G., Cowie, L. L., Barger, A., & Burke, D. J. 2002, AJ, 124, 1258
Yan, L., et al. 1999, ApJ, 519, L47
Zehavi, I., et al. 2004, ApJ, 608, 16
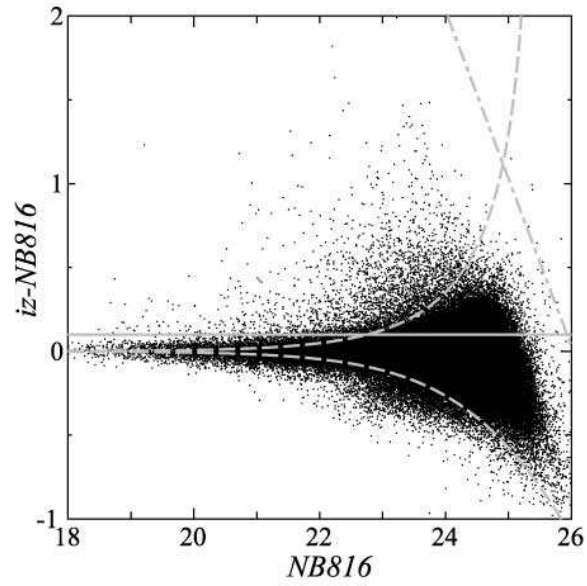Zehavi, I., et al. 2005, ApJ, 630, 1

FIG. 1.— Diagram of $iz-NB816$ vs. $NB816$ for all objects classified as galaxies in the ACS catalog. The horizontal solid line corresponds to $iz-NB816=0.1$. The dashed lines show the distribution of 3σ error. the dot-dashed line shows the limiting magnitude of iz. Since the total i'-magnitudes of galaxies in the official photometric redshift catalog are brighter than 25, iz magnitudes of most of them are brighter than the limiting magnitude.
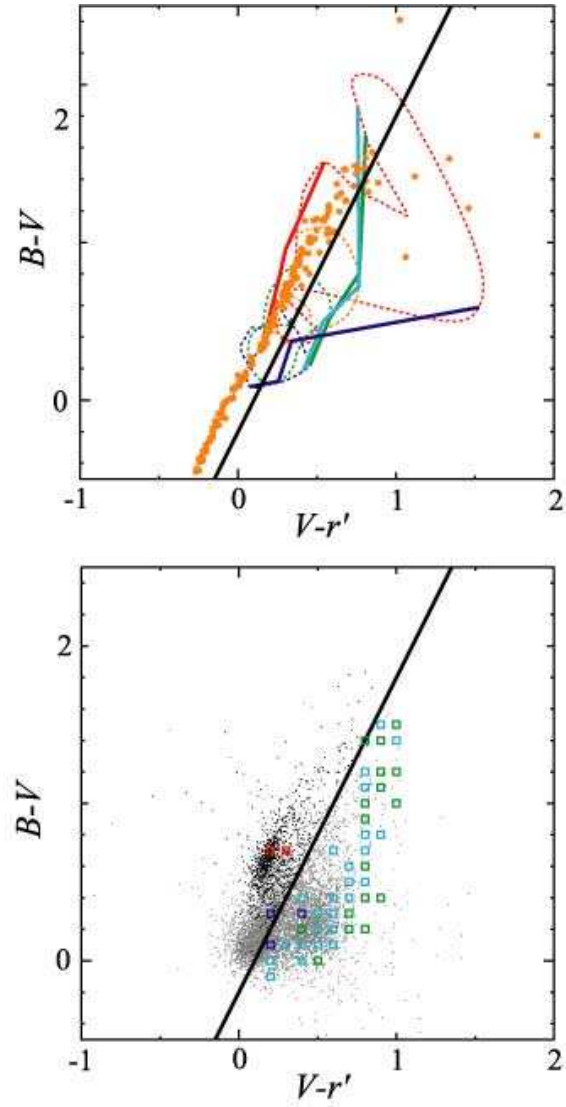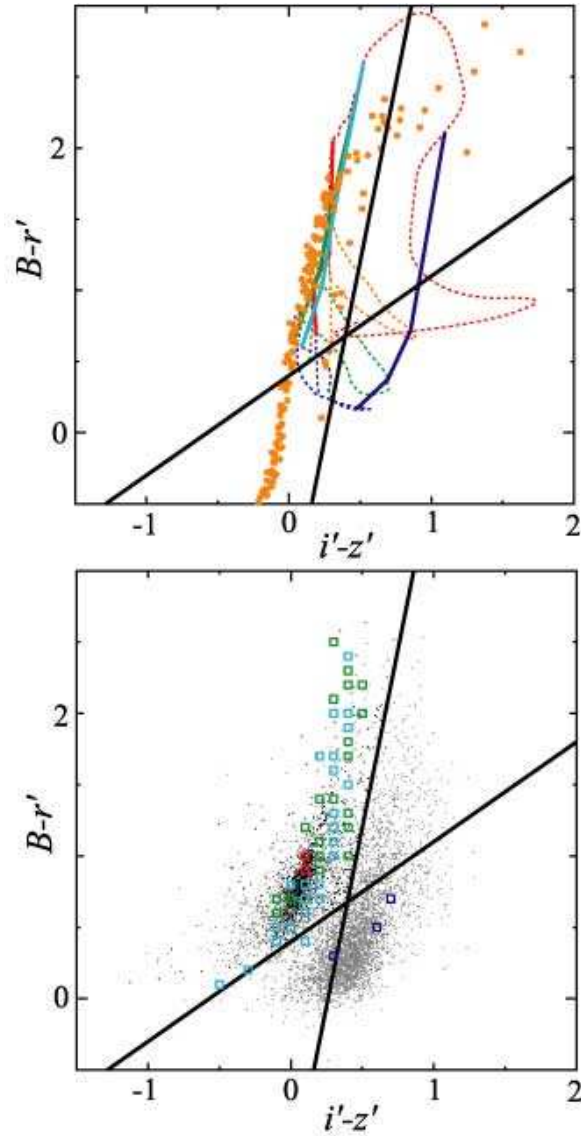
FIG. 2.— Diagrams between $B - V$ vs. $V - r'$. *Top*: Colors of model galaxies (CWW) from $z = 0$ to $z = 3$ are shown with dotted lines: red, orange, green, and blue lines show the loci of E, Sbc, Scd, and Irr galaxies, respectively. Colors of $z = 0.24$, 0.64, 0.68, and 1.18 (for Hα, [O III], Hβ, and [O II] emitters, respectively) are shown with red, green, light blue, and blue lines, respectively. Orange asterisks show Gunn and Stryker (1983)'s star. *Bottom*: Plot of $B - V$ vs. $V - r'$ for the 6176 sources found with emitter selection criteria. In this diagram, Hα emitters are located above the black line, that is adopted by us as one of the criteria for the selection of Hα emitters. The 980 Hα emitters are shown as black dots and other emission-line galaxy candidates are shown by gray dots. Galaxies in GOODS-N (Cowie et al. 2004) with redshifts corresponding to Hα emitters, [OIII] emitters, Hβ emitters and [OII] emitters are shown as red, green, light blue and blue open squares, respectively.

FIG. 3.— Diagrams between $B - r'$ vs. $i' - z'$. *Top*: Colors of model galaxies (CWW) from $z = 0$ to $z = 3$ are shown with dotted lines: red, orange, green, and blue lines show the loci of E, Sbc, Scd, and Irr galaxies, respectively. Colors of $z = 0.24$, 0.64, 0.68, and 1.18 (for Hα, [O III], Hβ, and [O II] emitters, respectively) are shown with red, green, light blue, and blue lines, respectively. Orange asterisks show Gunn and Stryker (1983)'s star. *Bottom*: Plot of $B - r'$ vs. $i' - z'$ for the 6176 sources found with emitter selection criteria (black dots). In this diagram, Hα emitters are located above the both of black lines, that is adopted by us as one of the criteria for the selection of Hα emitters. The 980 Hα emitters are shown as black dots and other emission-line galaxy candidates are shown by gray dots. Galaxies in GOODS-N (Cowie et al. 2004) with redshifts corresponding to Hα emitters, [OIII] emitters, Hβ emitters and [OII] emitters are shown as red, green, light blue and blue open squares, respectively.
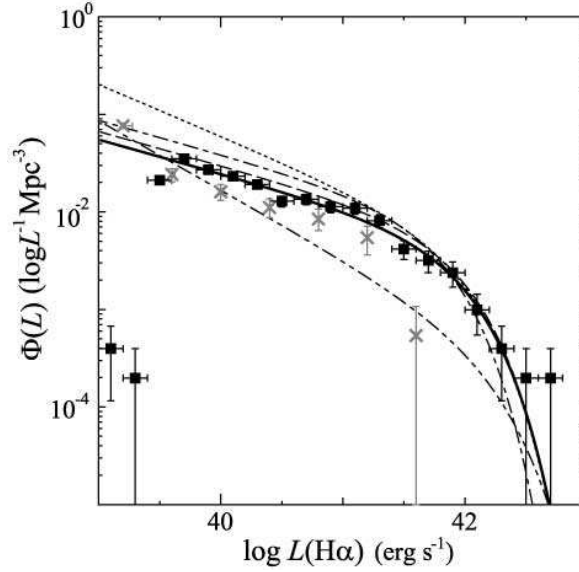
FIG. 4.— Our Hα luminosity function (filled squares and thick solid line) and Hα luminosity functions in previous works. The Tresse & Maddox (1998)'s Hα luminosity function at $z \leq 0.3$ is shown with the dashed line. The Hα luminosity functions derived by Fujita et al. (2003), Hippelein et al. (2003), and Ly et al. (2007) are shown with the dotted line, the dot-dashed line, and dashed and double-dotted line, respectively. Data points of Ly et al. (2007)'s Hα LF are shown as gray crosses.
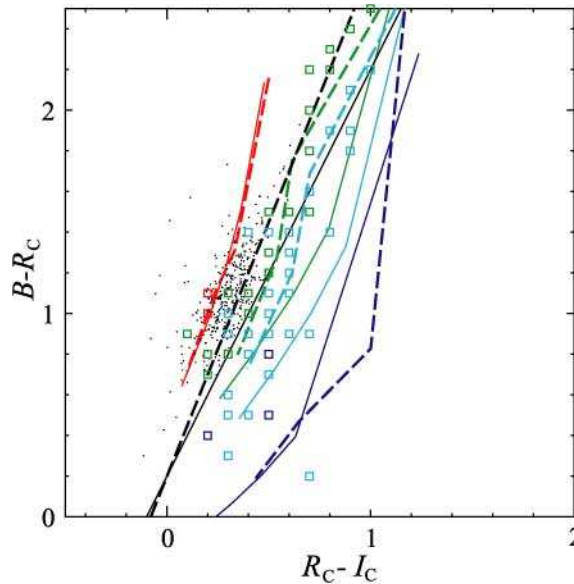

FIG. 5.— $B - R_C$ vs. $R_C - I_C$ color - color diagram of model galaxies. Colors of $z = 0.24$, 0.64, 0.68, and 1.18 (for Hα, [O III], Hβ, and [O II] emitters, respectively) are shown with red, green, light blue, and blue lines, respectively. The loci calculated by using GISSEL96 (Bruzual & Charlot 1993) are shown by solid lines and those calculated by using CWW are shown by dashed lines. Galaxies in GOODS-N (Cowie et al. 2004) with redshifts corresponding to Hα emitters, [OIII] emitters, Hβ emitters and [OII] emitters are shown as red, green, light blue and blue open squares, respectively. Fujita et al. (2003) selected galaxies above the black solid line as Hα emitter candidates. If we reselect Hα emitter candidates as sources above the black dashed line, some of the Hα emitter candidates (black dots) do not satisfy the new criterion.
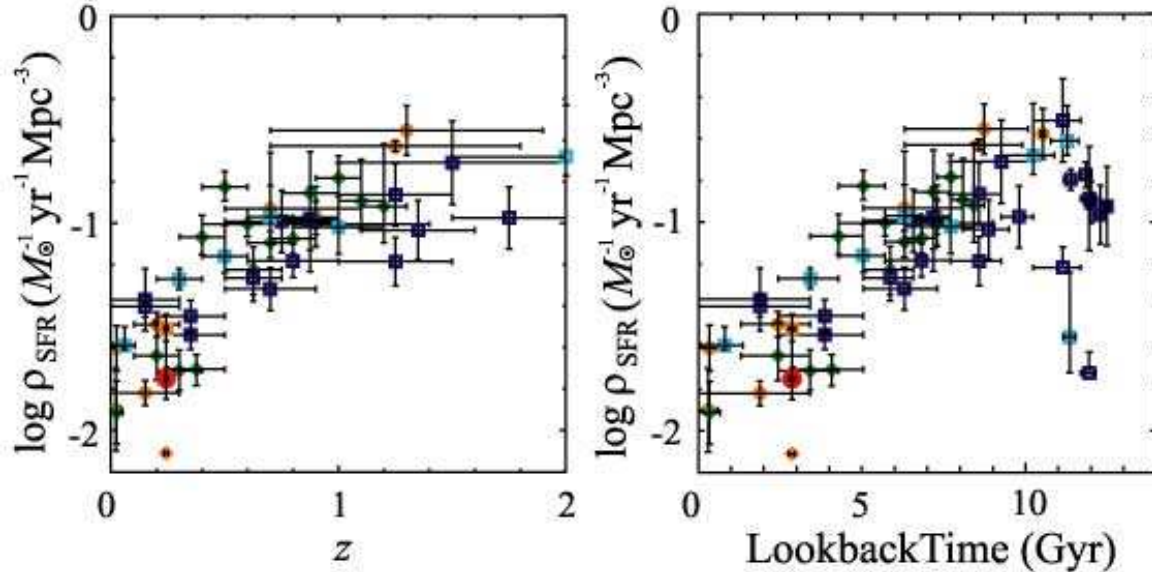
Fig. 6.— Star formation rate density (SFRD) at $z \approx 0.24$ derived from this study (large red filled circle) shown together with the previous investigations compiled by Hopkins (2004). SFRDs estimated from Hα, [O$_{II}$], and UV continuum are shown as orange open circles (Pérez-González et al. 2003; Tresse et al. 2002; Moorwood et al. 2000; Hopkins et al. 2000; Glazebrook et al. 1999; Yan et al. 1999; Tresse & Maddox 1998; Gallego et al. 1995), green open diamonds (Teplitz et al. 2003; Gallego et al. 2002; Hogg et al. 1998; Hammer et al. 1997), and blue squares (Wilson et al. 2002; Massarotti et al. 2001; Sullivan et al. 2000; Cowie et al. 1999; Treyer et al. 1998; Connolly et al. 1997; Lilly et al. 1996). The light blue open squares show SFRDs based on the UV luminosity density by Schiminovich et al. (2005), assuming $A_{\mathrm{FUV}} = 1.8$. An orange open square and an orange open diamond show SFRDs at $z \approx 0.24$ derived by Fujita et al. (2003) and Ly et al. (2007), respectively. In the left panel, we show the evolution of SFRD as a function of redshift, and in the right panel, we show it as a function of lookback time.
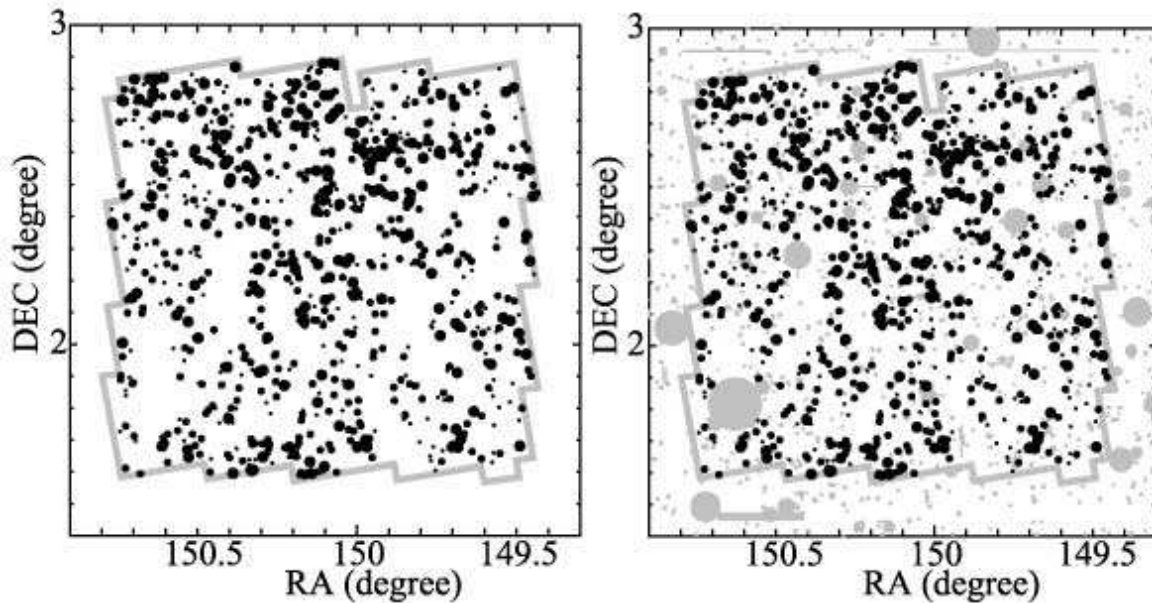

Fig. 7.— Spatial distributions of our H α emitter candidates (black filled circles and black dots). Gray open squares in the both panels show our survey area. The shadowed regions in the right panel show the areas masked out for the detection. We show the luminous Hα emitters [$\log L(\mathrm{H}\alpha)(\mathrm{erg\ s}^{-1}) > 40.94$] as large filled circles and the faint Hα emitters [$39.8 < \log L(\mathrm{H}\alpha)(\mathrm{erg\ s}^{-1}) \le 40.94$] as small filled circles. Hα emitters with $\log L(\mathrm{H}\alpha)(\mathrm{erg\ s}^{-1}) \le 39.8$ are shown as black dots.
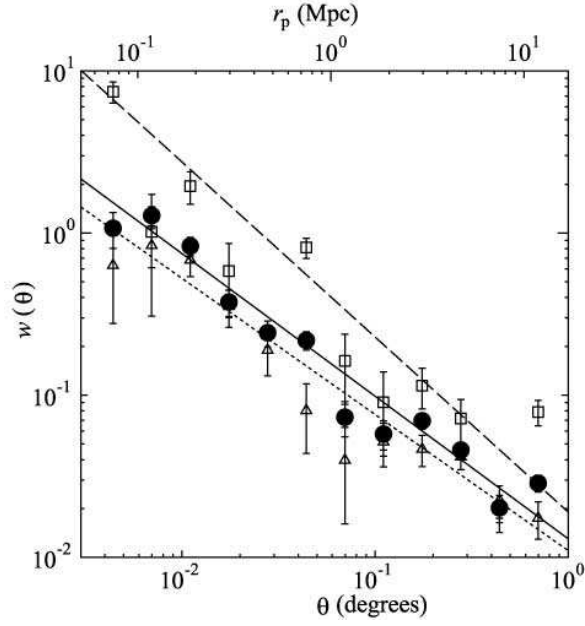
Fig. 8.— Angular two-point correlation function of all H α emitter candidates (filled circles), bright Hα emitter candidates ($\log L(\mathrm{H}\alpha)(\mathrm{erg\ s}^{-1}) > 40.94$: open squares), and faint Hα emitter candidates ($39.8 < \log L(\mathrm{H}\alpha)(\mathrm{erg\ s}^{-1}) \leq 40.94$: open triangles). Solid line shows the relation of $w(\theta) = 0.013\theta^{-0.88}$. Dashed line shows the best-fitting power law for bright ones, $w(\theta) = 0.019\theta^{-1.08}$, and dotted line shows that for faint ones, $w(\theta) = 0.011\theta^{-0.84}$.
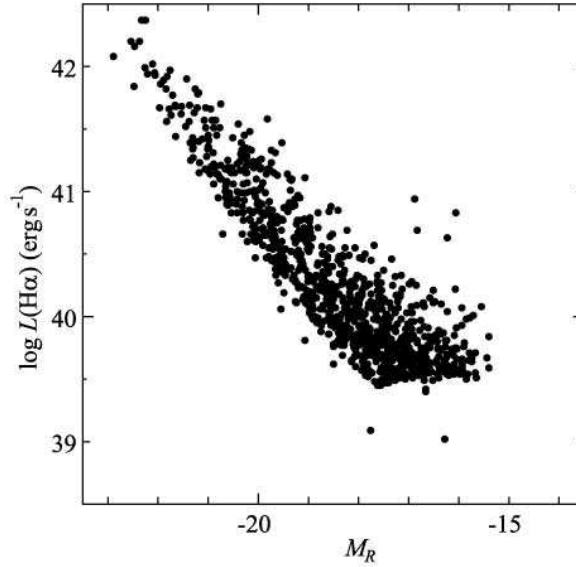

Fig. 9.— Relation between Hα luminosities and R-band absolute magnitudes for our Hα emitters.